Synthesis and Characterization of Ferrocene Containing Block Copolymers

Sergey Chernyy,[1] Zhongli Wang,[1,2] Jacob Judas Kain Kirkensgaard,[3] Anders Bakke,[3] Kell Mortensen,[3] Sokol Ndoni,[1,2] Kristoffer Almdal[1,2]

[1]DTU Nanotech – Department of Micro- and Nanotechnology, Technical University of Denmark, Produktionstorvet, 2800 Kgs. Lyngby, Denmark
[2]DTU Nanotech – Department of Micro- and Nanotechnology, Center for Nanostructured Graphene, CNG, Produktionstorvet, 2800 Kgs. Lyngby, Denmark
[3]Niels Bohr Institute, University of Copenhagen, Copenhagen 2100, Denmark
Correspondence to: S. Chernyy (E-mail: sergeychernyy@gmail.com)

Received 16 September 2016; accepted 1 November 2016; published online 22 November 2016
DOI: 10.1002/pola.28435

ABSTRACT: Narrowly dispersed diblock copolymers containing poly(methyl methacrylate) [PMMA] or poly(nonafluorohexyl methacrylate) [PF9MA] as the first block and poly(ferrocenylmethyl methacrylate) [PFMMA] as the second block, were prepared by anionic polymerization for the first time. Disordered bulk morphologies in the case of PMMA-*b*-PFMMA were observed and explained in terms of low Flory–Huggins interaction parameter ($\chi \leq 0.04$). In the case of PF9MA-*b*-PFMMA hexagonally packed cylinder morphology (HEX) was substantiated from TEM and SAXS observations. Furthermore, high incompatibility between PF9MA and PFMMA blocks allowed for the formation of well-ordered ferrocene containing cylinders on silica substrate upon exposure of the thin films to a saturated solvent vapor. It was shown that the cylinder orientation, parallel or perpendicular to the surface, could easily be controlled by appropriate choice of the solvent and without the need for preliminary surface modification, for example by means of grafted brush layer. © 2016 Wiley Periodicals, Inc. J. Polym. Sci., Part A: Polym. Chem. **2017**, *55*, 495–503

KEYWORDS: anionic polymerization; diblock copolymers; ferrocenylmethyl methacrylate (FMMA); Flory–Huggins interaction parameter; 1*H*,1*H*,2*H*,2*H*-nonafluorohexyl methacrylate (F9MA); order–disorder transition; rheology

INTRODUCTION Ferrocene-based polymers are attractive due to such valuable metallocene-rendered properties as low toxicity, excellent one electron redox reversibility,[1] magnetic susceptibility,[2–4] photo- and semiconductivity,[5–9] ability to form polymeric charge-transfer complexes,[10,11] to quench triplet states,[11] and so forth. More specifically, the presence of organoiron moieties in the main polymer chain or in the side groups infer high glass transition temperature (T_g) of the resulting polymers mainly due to the high cohesive energy density of the ferrocenyl groups.[11] The high T_g of ferrocene-containing polymers combined with their excellent plasma etch selectivity could be beneficial for, for example, block copolymer lithography applications allowing for pattern formation at high temperatures.[12,13] Moreover, the ability of ferrocene containing polymers to switch between II and III oxidation states was recently employed to create stimuli-responsive diblock copolymers and a controlled release of encapsulated compounds from poly(vinylferrocene)-*b*-poly(methyl methacrylate) [PVFc-*b*-PMMA] based micelles have been achieved by reversible oxidation of ferrocene to stable ferrocenium (ferricenium) cations.[14–16]

Most of the ferrocene containing polymers are currently produced by living anionic polymerization, RAFT, ATRP, or free radical polymerization techniques. In the latter case the peroxide-based free radical initiators should be excluded due to their possible reduction by ferrocene moieties resulting in low conversions. We selected anionic polymerization for the synthesis of diblock copolymers of ferrocenylmethyl methacrylate (FMMA) and methyl methacrylate (MMA) or FMMA and 1*H*,1*H*,2*H*,2*H*-nonafluorohexyl methacrylate (F9MA), with the aim to further investigate the bulk and surface morphologies of the resulting novel block copolymers by means of TEM, SEM, SAXS, Rheology, and AFM.

To the best of our knowledge, no well-ordered morphologies for PFMMA containing diblock copolymers were reported in the up-to-date literature. Resent work by Gallei et al. on poly (styrene) [PS] block copolymers with PFMMA (PS-*b*-PFMMA)

Additional Supporting Information may be found in the online version of this article.

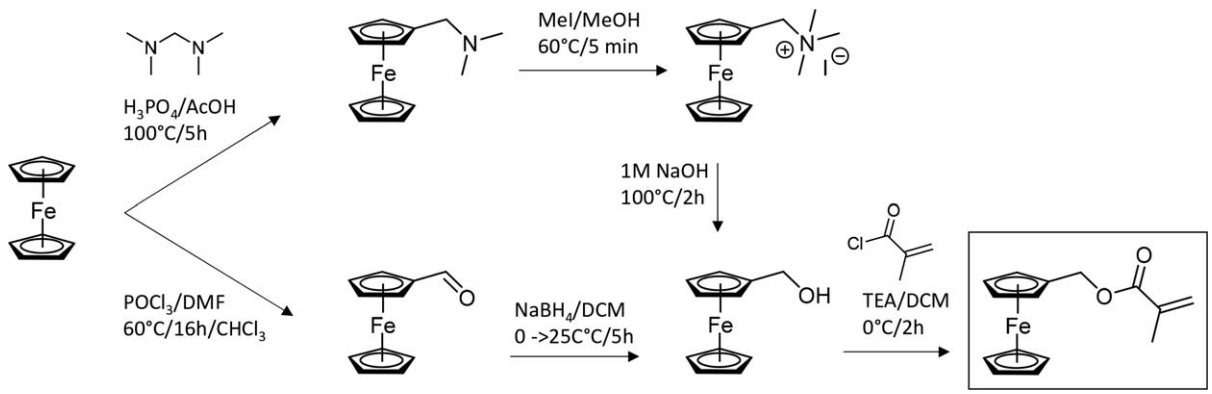

SCHEME 1 Synthesis of ferrocenylmethyl methacrylate (FMMA).

concludes that incomplete phase separation of PS and PFMMA blocks takes place presumably due to their good mutual compatibility.[17] Cylindrical, spherical, and lamellar morphologies for poly(ferrocenyldimethylsilane-*b*-dimethylsiloxane) (PFS-b-PDMS) and PS-b-PFS diblock copolymers of various composition were reported.[4] Also, micellization of poly(isoprene-*b*-ferrocenylmethylsilane) (PI-*b*-PFMS) and PFS-*b*-PI was recently investigated.[18,19] Moreover, a complete overview of the synthesized polyferrocenylsilanes could be found in the excellent review by Manners and co-workers[20]

Thermodynamic incompatibility between the metallocene-containing block and the purely organic blocks was also assessed in the present work, although to a minor extent. Understanding the Flory–Huggins interaction parameter (χ) is important from both fundamental and application point of views since it allows to, for example, design patterns with predetermined pitch and size of the organoiron domains, estimate the minimum molecular weight for a given diblock copolymer needed to be able to undergo the microphase separation, chose the right monomer for the second block to minimize or maximize the sharpness of the boundary between the microphases in a diblock copolymer.[21]

EXPERIMENTAL

All chemicals were purchased from Sigma-Aldrich unless otherwise stated. Tetrahydrofuran (THF) was distilled from ketyl radical of benzophenone under argon. Methyl methacrylate (MMA) was consecutively distilled from calcium hydride (CaH_2) and triethylaluminum ($AlEt_3$). Attempts to distill 1*H*,1*H*,2*H*,2*H*-nonafluorohexyl methacrylate (F9MA, TCI) from $AlEt_3$ were not successful due to onset of rapid polymerization; instead, F9MA was distilled twice from CaH_2.

The molecular weight was determined by gel permeation chromatography (GPC) using THF with 1% triethylamine as an eluent at 0.5 ml/min flow rate with a column set consisting of a precolumn and two 300 × 8 mm main columns (PLgel Mixed C and Mixed D). Transmission electron microscopy (TEM) was performed on microtomed samples (60 nm thick) without staining using FEI Tecnai T20 G^2 at 200 kV in a bright field mode. For scanning electron microscopy (SEM) of the microphases on silica substrates a Zeiss Supra 40VP was used at 3 kV accelerating voltage and 3–4 mm working distance. X-ray photoelectron spectroscopy (XPS) data were acquired on ThermoScientific XPS instrument equipped with an Al K-Alpha source of 1486 eV energy. Samples were analyzed using charge compensation from a flood gun in a vacuum not exceeding 10^{-7} mbar with a spot size of 400 × 400 μm. Rheological characterization was realized on a Rheometrics solids analyzer (RSA II) operated with a 0.3 mm gap shear sandwich configuration at 1% shear strain (γ) amplitude and 1 rad/s frequency (ω). Small-angle X-ray scattering (SAXS) profiles were measured using the SAXSLab instrument at the Niels Bohr Institute (NBI). The SAXSLab instrument uses a Rigaku 40W micro-focused Cu-source producing X-rays with a wavelength of 1.54 Å which is detected by a moveable Pilatus 300k pixel-detector. A sample was mounted in small Cu-discs between two 5–7 μm mica windows. The *q* calibration of the instrument was done by using silver behenate as a reference.

N,N-dimethylaminomethylferrocene[22,23]

N,N-dimethylaminomethylferrocene was synthesized via aminomethylation of ferrocene with *N,N,N′,N′*-tetramethylmethylenediamine (Scheme 1). In a typical run, ferrocene (46.4 g, 0.25 mol) was added to the stirred mixture of *N,N,N′,N′*-tetramethylmethylenediamine (43.2 g, 0.42 mol), H_3PO_4 (43.2 g, 0.44 mol) and acetic acid (400 ml, 6.99 mol). The mixture color turned to dark amber upon heating to 100 °C for 5 h (oil bath). The mixture was cooled to room temperature, diluted with water and neutralized with 275 g NaOH while cooling with ice. After the extraction with diethyl ether the ethereal fractions were combined, three times washed with water, dried over Na_2SO_4 and concentrated on a rotary evaporator. Distillation of the product under reduced pressure afforded 36.3 g of *N,N*-dimethylaminomethylferrocene as a dark-red mobile liquid, yield 61%. ^{1}H NMR ($CDCl_3$, 400 MHz, in ppm): 4.10 (m, 6H), 3.26 (d, $J = 8.9$ Hz, 2H), 2.16 (d, $J = 1.9$ Hz, 6H).

N,N-Dimethylaminomethylferrocene Methiodide[23]

Methyl iodide (37.0 g, 0.26 mol) was added dropwise to the solution of *N,N*-dimethylaminomethylferrocene (36.3 g, 0.15 mol) in 50 ml methanol. The mixture was refluxed for 5 min

followed by addition of 400 ml diethyl ether. The resulting yellow crystals were filtered and dried affording 57 g of the product, yield 97%. ^{1}H NMR ($CDCl_3$, 400 MHz, in ppm): 4.90 (s, 2H), 4.57 (m, 2H), 4.34 (m, 2H), 4.30 (s, 5H), 3.31 (s, 9H).

Ferrocenecarboxaldehyde[24]

$POCl_3$ (75 ml, 0.8 mol) was added slowly to dimethylformamide (150 ml, 1.95 mol) while cooling with ice. After 15 min the mixture was diluted with 200 ml of chloroform and ferrocene (50 g, 0.27 mol) was added. The dark amber mixture was stirred at 60 °C for 16 h. Ice water (1 L) was slowly added to the cooled reaction mixture followed by 70 g of NaOH and 215 g of sodium acetate. The product was extracted with 1L of chloroform, washed three times with water and concentrated. The tar was removed by flushing the product though a silica column (hexane:acetone 5:1) affording 35 g of crimson crystals, yield 61%. ^{1}H NMR ($CDCl_3$, 400 MHz, in ppm): 9.95 (s, 1H), 4.79 (s, 2H), 4.60 (s, 2H), 4.27 (s, 5H).

Ferrocenemethanol from *N,N*-Dimethylaminomethylferrocene Methiodide[23]

A solution of sodium hydroxide (1 M, 500 ml, 0.5 mol) was added to *N*,*N*-dimethylaminomethylferrocene methiodide (57 g, 0.15 mol). The resulting slurry was refluxed at 110 °C (oil bath) for 2 h, cooled to room temperature and acidified with 45 ml of 37% HCl diluted in 100 ml of water. $NaHCO_3$ was slowly added until neutral pH. The mixture was extracted with 1 L of dichloromethane and concentrated. Recrystallization of the crude product from hexane afforded 15 g of highly pure (TLC) hydroxymethyl ferrocene in a form of yellow needles, yield 47%. ^{1}H NMR ($CDCl_3$, 400 MHz, in ppm): 4.31 (s, 2H), 4.28 (s, 2H), 4.24 (s, 7H), 1.47 (s, 1H).

Ferrocenemethanol from Ferrocenecarboxaldehyde[17]

To the solution of ferrocenecarboxaldehyde (29.0 g, 0.14 mol) in 900 ml methanol $NaBH_4$ (13.5 g, 0.36 mol) was added within 2 h at 0 °C. Slightly brown mixture was warmed up to room temperature and stirred for additional 3 h. 1 L of saturated NH_4Cl solution was added resulting in a yellow-brown slurry. After 16 h the product was extracted with 800 ml (4 × 200 ml) dichloromethane, washed three times with 300 ml water, dried over Na_2SO_4 and concentrated affording 28.5 g of the ferrocenemethanol, yield 97%. ^{1}H NMR ($CDCl_3$, 400 MHz, in ppm): 4.31 (s, 2H), 4.28 (s, 2H), 4.24 (s, 7H), 1.47 (s, 1H).

Ferrocenylmethyl Methacrylate (FMMA)[25,26]

Methacryloyl chloride (16 ml, 0.16 mol) in 100 ml of dry dichloromethane (DCM) was added dropwise to the mixture of dry triethylamine (25 ml, 0.18 mol) and ferrocenemethanol (23.2 g, 0.11 mol) in 400 ml of dry DCM. The reaction mixture was stirred for 2 h at 0 °C and then 2 h at room temperature. The precipitant was filtered and DCM fraction was washed with 200 ml of the saturated $NaHCO_3$, 200 ml of brine and water (10 × 200 ml), dried over Na_2SO_4 and concentrated on rotary evaporator at 30 °C in the dark. Addition of 10 ml of hexane to the dark red liquid initiated crystallization of the product. After 1 day at +4 °C 22.5 g of FMMA was recovered in a form of bright orange crystals, yield 74%. ^{1}H NMR ($CDCl_3$, 400 MHz, in ppm): 6.11 (m, 1H), 5.55 (m, 1H), 4.96 (s, 2H), 4.29 (m, 2H), 4.18 (m, 7H), 1.95 (s, 3H).

Anionic Polymerization

The polymerizations were realized using a procedure described elsewhere.[27] Briefly, for the synthesis of PMMA-*b*-PFMMA diblock copolymer with a total molecular weight of 24 kDa, having a volume fraction of PFMMA block of 55%, abbreviated further as $PM_{24k}F_{55}$, the following step sequence was adopted. A solution of MMA (0.7 g) in THF was added to the mixture of sBuLi-DPE initiator (0.062 mmol) and LiCl (0.31 mmol, 5× relative to initiator) in 200 ml THF at −78 °C. After 1 h a THF solution of 0.8 g FMMA was added. After additional 1 h the living chains were terminated with 2 ml of degassed MeOH and the mixture was precipitated into 0.5 L of isopropanol followed by filtration and drying at 80 °C for 16 h at 1e-3 mbar. Yellow solid product was thereby obtained in a quantitative yield (Scheme 2)

RESULTS AND DISCUSSION

The synthesis of FMMA monomer was realized in two different approaches (Scheme 1). In Route 1, the initial ferrocene was aminomethylated and the introduced dimethylamino group was subsequently quaternized and hydrolysed affording the precursor compound, ferrocenemethanol.[22,23] In the second route, ferrocene was converted to ferrocenecarboxaldehyde in Vilsmeier-Haak formylation conditions and aldehyde group was mildly reduced to alcohol giving the same ferrocenemethanol precursor.[17,24,28] Finally, by acylation of ferrocenemethanol with methacryloyl chloride the targeted FMMA was produced.[25,26] The second route appears to be more attractive due to reduced number of steps required and commercial availability of the ferrocenecarboxaldehyde, which would further shorten the time required for the synthesis.

Block copolymer synthesis was realized by sequential addition of the monomers to the initiator solution. First, MMA was polymerized and then a solution of FMMA in THF was added to the living PMMA-Li chains. Such sequence was chosen because PMMA-Li chains are more nucleophilic than PFMMA-Li due to the stabilizing effect of ferrocenylmethyl substituent on forming carbanion.[29] For $PF9_{35k}F_{25}$ the sequence was inversed since the perfluoroalkyl substituent is expected to exert a higher electron withdrawing effect compared with the ferrocenylmethyl group. As a result, a series of block copolymers with molecular weights in the range 15–35 kDa and polydispersities 1.02–1.04 were successfully synthesized (Table 1).

TGA

The thermal stability of the synthesized block copolymers was found to be strongly dependent on the nature of the first block. In the case of PFMMA homopolymer, the temperature corresponding to the maximum rate of decomposition (T_{max}) is equal to 454 °C (Fig. 1). For the diblock copolymer

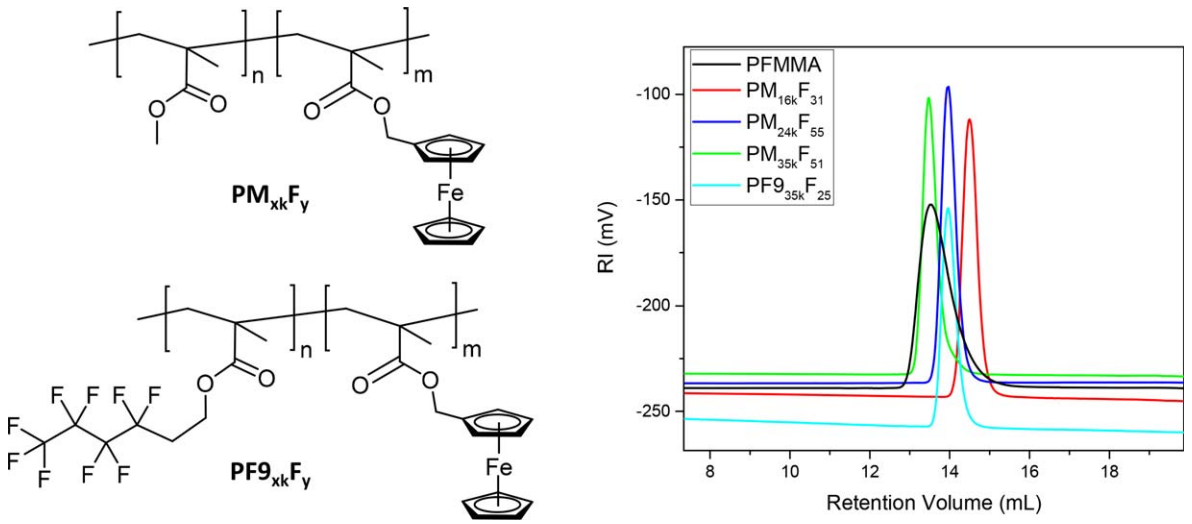

SCHEME 2 (left) chemical structures of the PMMA-*b*-PFMMA ($PM_{xk}F_y$) and PF9MA-*b*-PFMMA ($PF9_{xk}F_y$) diblock copolymers and (right) the corresponding GPC curves. In the name of the sample, the first subscript denotes total molecular weight of the diblock copolymer while the second subscript signifies the average (from NMR and TGA) volume fraction (in %) of the PFMMA block. [Color figure can be viewed at wileyonlinelibrary.com]

with PMMA stability decreases by 65–87 °C ($T_{max} = 389$ °C for $PM_{24k}F_{55}$ and 367 °C for $PM_{16k}F_{31}/PM_{35k}F_{51}$). Furthermore, a 187 °C decrease in stability ($T_{max} = 267$ °C) was observed for PF9MA containing diblock copolymer presumably due to facile formation of nonafluorohex-1-ene and cyclic esters upon PF9MA block degradation.[30]

Furthermore, the residue after the thermal degradation of block copolymers in air was analyzed by means of XPS and was found to consist of pure Fe_2O_3 (Supporting Information, S1). By taking into account the molecular weight of the iron (III) oxide we can use the data on the TGA residue to calculate the volume fraction of the PFMMA block and therefore independently assess the composition of the block copolymer. As seen from the last two columns of Table 1, the volume fractions of PFMMA block (f_{PFMMA}) calculated from the TGA residues and by NMR are in good agreement.

Rheology

Isochronal temperature scans[31–33] for the poly(ferrocenylmethyl methacrylate) (PFMMA) homopolymer and diblock copolymers are presented in Figure 2. The dynamical mechanical spectrum of PFMMA is in general agreement with the data for low molecular weight uncrosslinked polymers.[34] The polymer behaves as a true viscoelastic solid up to 160 °C since the elasticity ($\sim G'$) is higher than viscosity ($\sim G''$) whereas viscous behavior starts to dominate at higher temperatures. No rubbery plateau, expected to occur within 10^3-10^4 Pa, was detected after the softening indicating that the molecular weight of PFMMA (45.8 kDa) is lower that the double critical entanglement molecular weight ($2M_e$). Considering typical values of M_e for poly(styrene),that is 13–19 kDa,[27,35] we suggest that bulky ferrocenylmethyl substituents prevent the formation of intermacromolecular entanglements even at relatively high molecular weight of PFMMA (45.8 kDa). Above 210 °C PFMMA starts to be unstable and undergoes decomposition and crosslinking reactions which results in the increase of both G' and G''.

PMMA containing block copolymers of low molecular weight ($PM_{16k}F_{31}$ and $PM_{24k}F_{55}$) demonstrate similar transitions during the temperature ramp indicating the absence of the

TABLE 1 Characteristics of the Synthesized PFMMA Homopolymer and Block copolymers

Name[a]	MW, kDa (NMR)	DP 1st block[b]	DP PFMMA	PDI (GPC)	Residue at 900 °C, %	f_{PFMMA} (NMR)	f_{PFMMA} (TGA)
PFMMA	45.8	–	161	1.15	25.1	1.00	1.00
$PM_{16k}F_{31}$	15.5	103	19	1.03	9.5	0.31	0.31
$PM_{24k}F_{55}$	24.4	101	50	1.02	15.9	0.56	0.53
$PM_{35k}F_{51}$	35.2	149	71	1.04	14.2	0.54	0.47
$PF9_{35k}F_{25}$	35.2	81	26	1.03	6.1	0.25	0.25

[a] In the name of the sample the first subscript denotes total molecular weight of the diblock copolymer while the second subscript signifies the average (from NMR and TGA) volume fraction (in %) of the PFMMA block.

[b] Degree of polymerization of the first block.

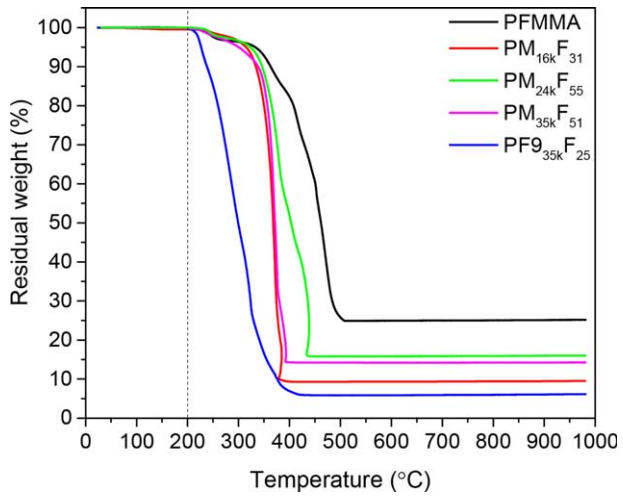

FIGURE 1 TGA curves of the synthesized block copolymers in air (flow = 60 ml/min) recorded at 10 °C/min heating rate. [Color figure can be viewed at wileyonlinelibrary.com]

ordered microphase separated morphologies. In the case of $PM_{35k}F_{51}$ sample, G' and G'' almost overlaps which could be explained by a decreased mobility of the chains in this relatively high molecular weight diblock copolymer.

On the contrary, $PF9_{35k}F_{25}$ sample of identical molecular weight undergoes microphase separation (ordering) below 140 °C as could be inferred from the higher values of G' compared with G''. The rearrangement of the chains during the transition process is facilitated by the low T_g of the PF9MA block (29 °C) [Supporting Information, S5] which imparts high chain mobility and fast relaxation processes. The formation of the ordered morphology is complete at 180 °C and the formed microstructure persists up to 220 °C due to high incompatibility between the blocks. Limited thermal stability precludes a direct observation of the order–disorder transition (segmental mixing) which is typically characterized by a sharp decrease of both G' and G'' to almost zero values. Overall, the characteristic rheological signature observed herein corresponds to the hexagonally packed cylinder morphology and it is in agreement with the literature reported rheological data[36] as well as SAXS (Supporting Information, S7) and TEM data (Fig. 3).

Different solubilities of the homopolymers from which a given diblock copolymer is composed could give an indirect indication of their mutual compatibility. We found that ethyl acetate, while being a good solvent for PMMA, swells but does not dissolve PFMMA. Such drastic difference in the solubility of two homopolymers is a positive indication of their mutual incompatibility. Sample $PM_{16k}F_{31}$ (PMMA-*b*-PFMMA) however has a disordered morphology, as discussed earlier. Low molecular weight of the constituent blocks (5–10.5 kDa) could explain this observation. For a given block copolymer the incompatibility of the blocks is characterized by a product of Flory–Huggins interaction parameter (χ) and the number of segments (N), χN. For a given composition, χ is constant (at constant temperature) and the immiscibility of two blocks could only be increased by producing higher molecular weight block copolymer to increase N.

The absolute χ value for PFMMA-*b*-PMMA is not known. For somewhat similar block copolymer of poly(styrene-*b*-ferrocenyldimethylsilane) [PS-*b*-PFDMS] the reported χ is equal to 0.032 at 150 °C which is almost identical to well-known weakly segregating PS-*b*-PMMA block copolymer ($\chi = 0.030$ at 150 °C).[21,37] Furthermore, the microphase separation in PS-*b*-PFMMA was shown to be incomplete due to considerable compatibility between PS and PFMMA.[17] It is thus reasonable to assume that PFMMA-*b*-PMMA would have very low incompatibility (if any) which necessitates the synthesis of high molecular weight polymer for verifying that assumption.

We therefore synthesized block copolymers having higher molecular weight. Samples $PM_{24k}F_{55}$ and $PM_{35k}F_{51}$ are clearly disordered, however, they have local composition fluctuations in a form of alternating dark (enriched with PFMMA) and bright (enriched with PMMA) areas (Fig. 3).

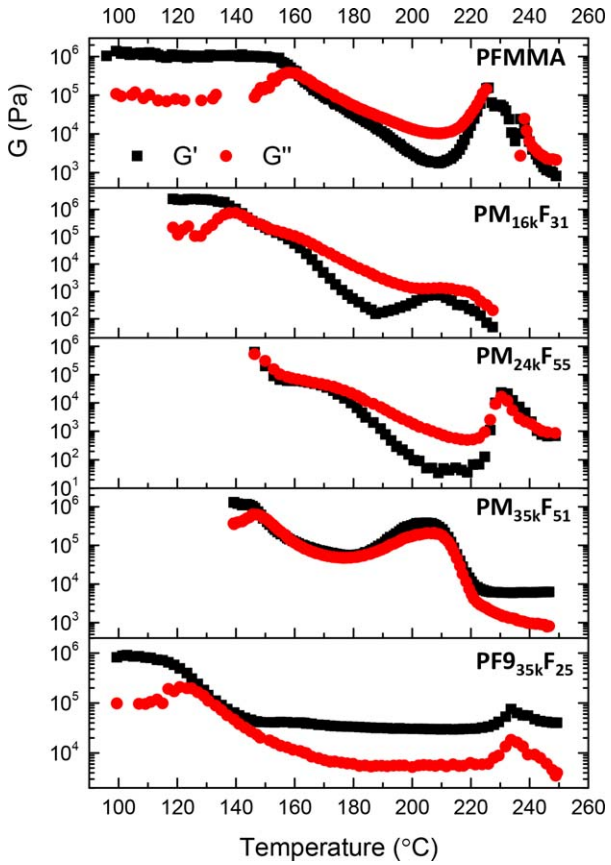

FIGURE 2 Isochronal ($\omega = 1$ rad/s) dynamic storage (G') and loss (G'') moduli measured at 2 °C/min heating rate and constant shear strain ($\gamma = 1\%$). The data below ca. 160 °C are not reliable due to instrumental limitations in measuring high modulus values and the transitions above ca. 200 °C are not reversible due to polymer degradation. [Color figure can be viewed at wileyonlinelibrary.com]

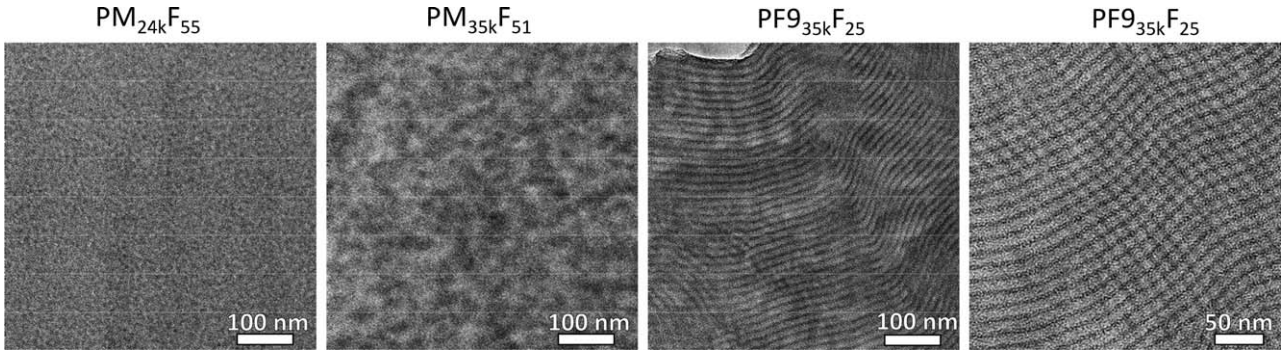

FIGURE 3 TEM images of the block copolymers. Samples were heat annealed at 160 °C for 65 h in vacuum then microtomed to 60 nm films and observed by TEM without staining.

The absence of the homogeneous segmentally mixed states characterized by $\chi N \ll 10$ for PFMMA-*b*-PMMA samples indicate that $\chi N \leq 10$ and therefore we can estimate the upper boundary for the χ value as described below.[38] For the sample of 24.4 kDa the molecular weights of PMMA and PFMMA blocks are 10.2 and 14.2 kDa (from NMR) which after division with the densities of PMMA (1.18 g/cm^3) and PFMMA (1.37 g/cm^3) yield the volumes of one mole of PMMA and PFMMA blocks (8683 and 10370 cm^3/mol, respectively). After division with Avogadro number the volumes of one PMMA and PFMMA blocks become equal to 14.4 and 17.2 nm^3, respectively. Taking into account the standard reference volume[21] of the statistical segment N (= 0.118 nm^3), the N_{PMMA} and N_{PFMMA} would be equal to 142 and 146 units, while the total N amounts to 268 units. Considering $\chi N \leq 10$ we estimate the upper boundary of the Flory–Huggins interaction parameter, that is, $\chi \leq 0.04$ for PMMA-*b*-PFMMA diblock copolymer of 24.4 kDa at 160 °C.

Surface Morphologies

Block copolymer self-assembly is a powerful platform for nanolithography. However, most of the block copolymer lithography processes need preliminary surface modification, including grafting of a neutral polymer brush layer onto the substrate to balance the surface interactions with two blocks of a given diblock copolymer.[39–41] Here, we present a procedure that could potentially simplify the main stream block copolymer lithography process.[42] $PF9_{35k}F_{25}$ copolymer was directly applied on silicon substrate without any pretreatment by spin-coating from 0.1 wt% toluene solution at 2000 rpm for 30 s to give a 12 nm thin film.

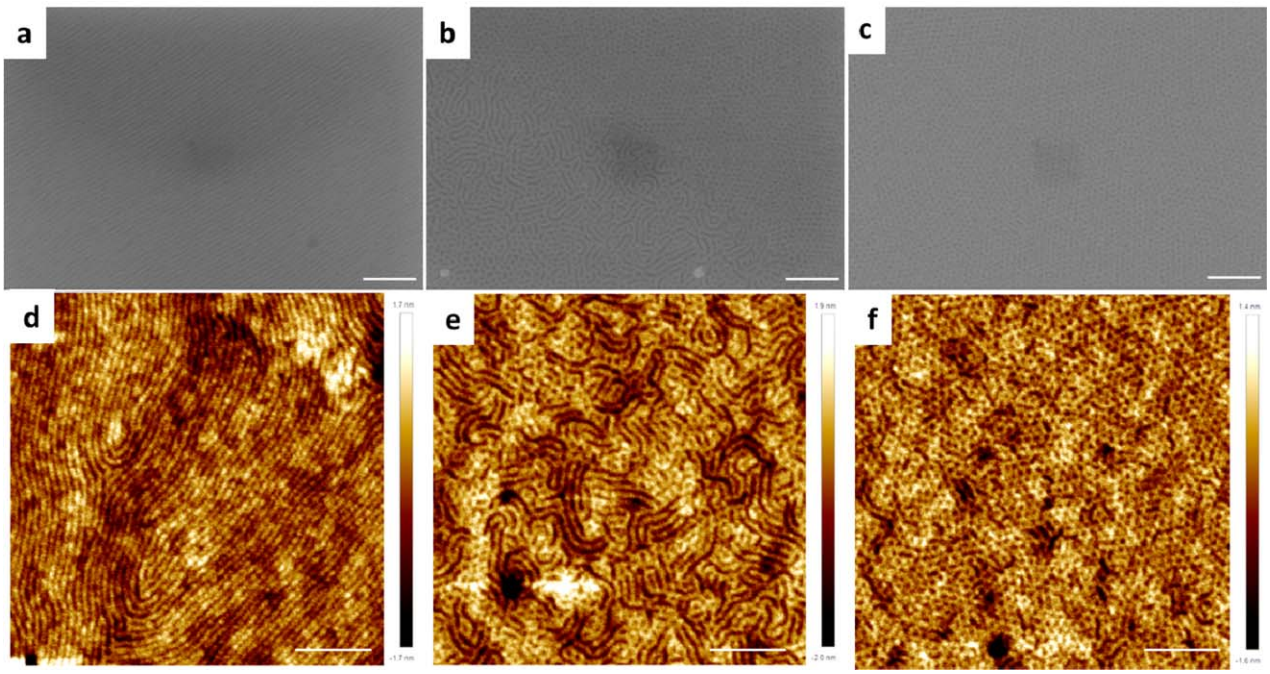

FIGURE 4 SEM (top-row) and AFM (bottom-row) images of $PF9_{35K}F_{25}$ on SiO_2/Si substrate after annealing for 20 min in (a, d) ethyl acetate atmosphere, (b, e) EA/THF atmosphere, and (c, f) THF atmosphere. Scale bars correspond to 100 nm. [Color figure can be viewed at wileyonlinelibrary.com]

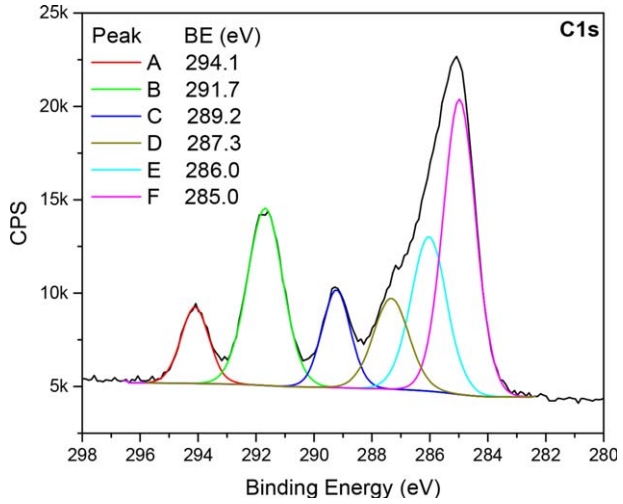

FIGURE 5 C1s HR XPS peak fitting for the $PF9_{35k}F_{25}$ thin film on silica substrate. [Color figure can be viewed at wileyonlinelibrary.com]

The morphologies formed at different conditions of solvent vapor annealing were investigated by SEM and AFM. Figure 4(a–c) shows top view SEM images of $PF9_{35k}F_{25}$ after three different conditions of annealing. The ordering behavior exhibits strong solvent dependence and the difference in the solubility of the PFMMA and PF9MA blocks gives a possibility to further manipulate the domain size and separation distances in thin films.

A morphology of well-ordered lying cylinders with 19 nm period is clearly seen upon annealing in saturated solvent vapor of ethyl acetate for 20 min (Fig. 4). The 19 nm period is in a good agreement with an equilibrium domain spacing (d) which was estimated by SAXS to be equal to 19.3 nm. This observation points out to the fact that the polymer chains forming cylinders parallel to the surface are in non-frustrated state.[43] When ethyl acetate/THF (v/v = 5/1) mixture was used for the solvent annealing for 20 min, a mixed morphology containing cylinders of both parallel and perpendicular orientations was observed [Fig. 4(b,e)]. Furthermore, well-ordered hexagonally packed cylinders perpendicular to the substrate surface were observed when the film was annealed in pure THF vapor for 20 min [Fig. 4(c,f)]. The reason for the change in the orientation of morphologies in different annealing solvent vapors can be explained in terms of the difference in solvent selectivity and solvent saturated vapor pressure.[44] The perpendicular orientation of HEX morphology requires the underlying surface to be neutral. Since ethyl acetate only swells but does not dissolve the PFMMA block it could be considered a more selective solvent for the PF9MA block. Therefore, in the presence of a selective solvent (ethyl acetate) the surface interactions are screened to a larger extent for PF9MA block but not for PFMMA block and, thus, specific adsorption of the PFMMA onto the substrate induces parallel cylinder orientation. On the contrary, when nonspecific solvent is present (THF) both blocks are well solvated, their mutual segment-segment interactions become screened to a certain extent while their surface interactions appear to be totally balanced ("neutral surface") resulting in the perpendicular with respect to the substrate orientation of the cylinders.

XPS

As to the elemental composition of the $PF9_{35K}F_{25}$ thin films, expected from the block copolymer structure C (45.5 At.%), O (10.6 At.%), F (38.3 At.%), and Fe (1.6 At.%) elements as well as small amount of Si (4.0 At.%) originating from the underlying substrate were found on the surface. Interestingly, the relative intensities and binding energies (BE) of C1s core electrons reflect the presence of six different carbon atoms containing substituents of varied polarity (Fig. 5) in high resolution (HR) XPS. The peak A at the highest BE 294.1 eV represents the most "electronegative" —CF_3 carbon and constitute 7% of the total C1s intensity which is in a good agreement with theoretically predicted 7% intensity. The prediction of the relative contributions from the six different carbons were made by taking into account the 3.09:1.00 PF9MA:FMMA monomer unit ratio in the $PF9_{35k}F_{25}$ block copolymer structure obtained from NMR. The peak B at 291.7 eV (20% vs. 21% theory) corresponds to the three —CF_2— atoms. The carbonyl C═O is located at 289.2 eV (9% vs. 9% theory) and has an equal contribution from the ester groups of two monomers. The D

TABLE 2 XPS Survey Data in Atomic Percents (At.%) for the PFMMA Films Before and After Exposure to Oxygen Plasma at Varied Pressure and Time

Time, min	Pressure, mbar	Si, At.%	C, At.%	O, At.%	Fe, At.%	C/Fe
Theory, PFMMA	–	0	83.3	11.1	5.6	15.0
0	0	0.0	81.9	11.3	6.8	12.1
1	1	0.0	40.0	45.0	15.0	2.7
2	1	0.0	38.2	45.6	16.3	2.3
5	1	0.0	32.2	49.7	18.1	1.8
10	1	0.0	26.5	54.3	19.2	1.4
1	0.36	0.0	25.2	54.5	20.3	1.2
2	0.36	9.9	11.2	58.1	20.8	0.5
5	0.36	11.1	13.4	57.0	18.5	0.7
10	0.36	20.0	10.5	54.8	14.6	0.7

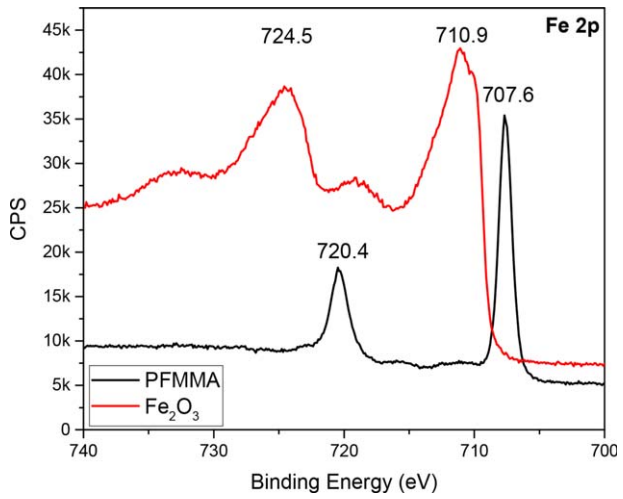

FIGURE 6 HR XPS spectra of Fe 2p for the PFMMA thin film (2 wt% in toluene, 3 krpm) before (black curve) and after (red curve) being exposed to oxygen plasma for 10 min (0.36 mbar, 50 W). [Color figure can be viewed at wileyonlinelibrary.com]

(16% vs. 11% theory) and E (15% vs. 19% theory) peaks at moderately low BE are typically ascribed to the carbon atoms with less polar substituents, such as —C—O—, tertiary carbons in the polymer backbone and tree carbons in the substituted cyclopentadienyl ring of the ferrocene. At last, the peak F (33% vs. 33% theory) could be unambiguously attributed to the $—CH_2—$, $—CH_3$ groups in the backbone and five —CH═ carbons of the unsubstituted cyclopentadienyl ring.[45–47]

Oxygen Plasma Etching

To demonstrate the concept of the plasma etch resistance of the ferrocene-containing polymers in general, we analyzed the etch selectivity of the PFMMA homopolymer (Table 2). By conducting the plasma etching at high pressure, we observe highly anisotropic etching and inefficient removal of the carbon from the organometallic block. Reducing the pressure ~3 times afforded higher ion energy[48] in the plasma which, in turn, facilitated physical sputtering and removal of the organic material from the layer. As a result, underlying silicon substrate becomes detectable by XPS already after 2 min of the oxygen plasma etching. Importantly, a significant amount of Fe remains on the surface and is not removed by oxygen plasma. By comparing the C/Fe ratio before and after 10 min etching at 0.36 mbar we estimated 17 times higher etch resistivity of the forming iron oxide with respect to the organic fraction of the PFMMA.

The presence of the iron (III) oxide was confirmed by high resolution (HR) XPS. Peaks at lower binding energy corresponding to the non-oxidized ferrocenylmethyl methacrylate (Fe $2p_{3/2} = 707.6$ and Fe $2p_{1/2} = 720.4$ eV) appear to be shifted to the higher binding energy corresponding to Fe_2O_3 (Fe $2p_{3/2} = 710.9$ and Fe $2p_{1/2} = 724.5$ eV, $\Delta = 13.6$ eV) after oxygen plasma treatment.[49–51] Also, appearance of the shake-up satellites characteristic for Fe_2O_3 is clear from Figure 6.[52]

CONCLUSIONS

The core findings of the work lend support to the following conclusions. Poly(methyl methacrylate) [PMMA] and poly(nonafluorohexyl methacrylate (PF9MA) diblock copolymers with poly(ferrocenylmethyl methacrylate) [PFMMA] could be produced solely by the anionic polymerization route affording well-defined products (PDI = 1.02–1.04). In the case of PMMA-*b*-PFMMA samples with molecular weight 16,000–35,000 g/mol, good compatibility ($\chi \leq 0.04$) between two blocks results in the absence of phase separation, as confirmed by rheology and TEM. On the contrary, when perfluorinated methacrylate was used in one of the blocks (PF9MA-*b*-PFMMA), the phase separation was easily attainable up to the degradation temperature of the diblock copolymer indicating high incompatibility. PFMMA homopolymer was shown to form F_2O_3 on the surface upon plasma etching which entails further applicability of the microphase separated thin films based on PF9MA-*b*-PFMMA copolymer. Such nanostructured films could potentially provide an access to either nanocylinders or nanodots of photoactive Fe_2O_3 on the substrate with high surface area and aspect ratio. These properties are highly desirable in the field of solar energy conversion.[53] We plan to further elaborate on the intriguing properties and applicability of ferrocene containing polymers in the upcoming publications.

ACKNOWLEDGMENTS

Authors are thankful to Villum Foundation for the financial support of the project. Support by the Danish National Research Foundation, Project DNRF103 is acknowledged. SC expresses gratitude to Niels B. Larsen for the helpful suggestions about plasma etching experiments.

REFERENCES AND NOTES

1 K. Tamura, N. Akutagawa, M. Satoh, J. Wada, T. Masuda, *Macromol. Rapid Commun.* **2008**, *29*, 1944–1949.

2 D. Posselt, W. Badur, M. Steiner, M. Baumgarten, *Synth. Met.* **1993**, *56*, 3299–3304.

3 M. Hmyene, A. Yassar, M. Escorne, A. Percheron-Guegan, F. Garnier, *Adv. Mater.* **1994**, *6*, 564–568.

4 J. A. Massey, K. N. Power, M. A. Winnik, I. Manners, *Adv. Mater.* **1998**, *10*, 1559–1562.

5 H. Yasuda, I. Noda, S. Miyanaga, A. Nakamura, *Macromolecules* **1984**, *17*, 2453–2454.

6 P. W. Cyr, M. Tzolov, I. Manners, E. H. Sargent, *Macromol. Chem. Phys.* **2003**, *204*, 915–921.

7 D. O. Cowan, J. Park, C. U. Pittman, Y. Sasaki, T. K. Mukherjee, N. A. Diamond, *J. Am. Chem. Soc.* **1972**, *94*, 5110–5112.

8 L. Espada, K. H. Pannell, V. Papkov, L. Leites, S. Bukalov, I. Suzdalev, M. Tanaka, T. Hayashi, *Organometallics* **2002**, *21*, 3758–3761.

9 L. Bakueva, E. H. Sargent, R. Resendes, A. Bartole, I. Manners, *J. Mater. Sci. Mater. Electron.* **2001**, *12*, 21–25.

10 A. S. Abd-El-Aziz, E. K. Todd, *Coord. Chem. Rev.* **2003**, *246*, 3–52.

11 C. U. Pittman, J. C. Lai, D. P. Vanderpool, M. Good, R. Prado, *Macromolecules* **1970**, *3*, 746–754.

12 I. Korczagin, R. G. H. Lammertink, M. A. Hempenius, S. Golze, G. J. Vancso, In Ordered Polymeric Nanostructures at Surfaces; G. J. Vancso, Ed.; Springer Berlin Heidelberg: Berlin, Heidelberg, **2006**; pp 91–117.

13 R. G. H. Lammertink, M. A. Hempenius, V. Z. H. Chan, E. L. Thomas, G. J. Vancso, *Chem. Mater.* **2001**, *13*, 429–434.

14 B. V. K. J. Schmidt, J. Elbert, C. Barner-Kowollik, M. Gallei, *Macromol. Rapid Commun.* **2014**, *35*, 708–714.

15 R. H. Staff, M. Gallei, M. Mazurowski, M. Rehahn, R. Berger, K. Landfester, D. Crespy, *ACS Nano* **2012**, *6*, 9042–9049.

16 M. Gallei, R. Klein, M. Rehahn, *Macromolecules* **2010**, *43*, 1844–1854.

17 M. Gallei, B. V. Schmidt, R. Klein, M. Rehahn, *Macromol. Rapid Commun.* **2009**, *30*, 1463–1469.

18 V. A. Du, H. Qiu, M. A. Winnik, G. R. Whittell, I. Manners, *Macromol. Chem. Phys.* **2016**, *217*, 1671–1682.

19 D. W. Hayward, G. R. Whittell, J. B. Gilroy, I. Manners, R. M. Richardson, *Liq. Cryst.* **2016**, *43*, 1148–1159.

20 R. L. N. Hailes, A. M. Oliver, J. Gwyther, G. R. Whittell, I. Manners, *Chem. Soc. Rev.* **2016**, *45*, 5358–5407.

21 C. Sinturel, F. S. Bates, M. A. Hillmyer, *ACS Macro Lett.* **2015**, *4*, 1044–1050.

22 D. Lednicer, C. R. Hauser, *Org. Synth.* **1960**, *40*, 31–33.

23 J. K. Lindsay, C. R. Hauser, *J. Org. Chem.* **1957**, *22*, 355–358.

24 J. Jia, Y. Cui, Y. Li, W. Sheng, L. Han, J. Gao, *Dyes Pigm.* **2013**, *98*, 273–279.

25 J. C. Lai, T. D. Rounsefell, C. U. Pittman, *Macromolecules* **1971**, *4*, 155–161.

26 R. W. Nguema Edzang, M. Lejars, H. Brisset, J. M. Raimundo, C. Bressy, *RSC Adv.* **2015**, *5*, 77019–77026.

27 M. F. Schulz, A. K. Khandpur, F. S. Bates, K. Almdal, K. Mortensen, D. A. Hajduk, S. M. Gruner, *Macromolecules* **1996**, *29*, 2857–2867.

28 G. Broadhead, J. Osgerby, P. Pauson, *J. Chem. Soc. (Resumed)* **1958**, 650–656.

29 Y. Matsuo, T. Oie, R. Goseki, T. Ishizone, K. Sugiyama, A. Hirao, *Macromol. Symp.* **2013**, *323*, 26–36.

30 A. Böker, K. Reihs, J. Wang, R. Stadler, C. K. Ober, *Macromolecules* **2000**, *33*, 1310–1320.

31 J. Zhao, B. Majumdar, M. F. Schulz, F. S. Bates, K. Almdal, K. Mortensen, D. A. Hajduk, S. M. Gruner, *Macromolecules* **1996**, *29*, 1204–1215.

32 S. Foerster, A. K. Khandpur, J. Zhao, F. S. Bates, I. W. Hamley, A. J. Ryan, W. Bras, *Macromolecules* **1994**, *27*, 6922–6935.

33 J. L. Adams, W. W. Graessley, R. A. Register, *Macromolecules* **1994**, *27*, 6026–6032.

34 G. Wilbert, A. Wiesemann, R. Zentel, *Macromol. Chem. Phys.* **1995**, *196*, 3771–3788.

35 J. Brandrup, E. H. Immergut, E. A. Grulke, A. Abe, D. R. Bloch, Polymer Handbook, 4th ed.; John Wiley & Sons, New York, **2003**; p. 2336.

36 M. Cloitre, D. Vlassopoulos, In Applied Polymer Rheology; John Wiley & Sons, Inc., **2011**; pp. 209–239.

37 H. B. Eitouni, N. P. Balsara, H. Hahn, J. A. Pople, M. A. Hempenius, *Macromolecules* **2002**, *35*, 7765–7772.

38 F. S. Bates, *Science* **1991**, *251*, 898–905.

39 M. Park, C. Harrison, P. M. Chaikin, R. A. Register, D. H. Adamson, *Science* **1997**, *276*, 1401–1404.

40 J. Bang, U. Jeong, D. Y. Ryu, T. P. Russell, C. J. Hawker, *Adv. Mater.* **2009**, *21*, 4769–4792.

41 J. N. L. Albert, T. H. Epps Iii, *Mater. Today* **2010**, *13*, 24–33.

42 T. Li, Z. Wang, L. Schulte, S. Ndoni, *Nanoscale* **2016**, *8*, 136–140.

43 M. J. Fasolka, P. Banerjee, A. M. Mayes, G. Pickett, A. C. Balazs, *Macromolecules* **2000**, *33*, 5702–5712.

44 W. A. Phillip, M. A. Hillmyer, E. L. Cussler, *Macromolecules* **2010**, *43*, 7763–7770.

45 J. F. Watts, *Surf. Interface Anal.* **1993**, *20*, 1–267.

46 S. Chernyy, S. Ulah, G. Sørensen, S. W. Tordrup, P. B. Pedersen, K. Almdal, *J. Appl. Polym. Sci.* **2015**, *132*, 41955(1-9).

47 S. Chernyy, B. E. B. Jensen, K. Shimizu, M. Ceccato, S. U. Pedersen, A. N. Zelikin, K. Daasbjerg, J. Iruthayaraj, *J. Colloid Interface Sci.* **2013**, *404*, 207–214.

48 M. A. Hartney, D. W. Hess, D. S. Soane, *J. Vac. Sci. Technol. B* **1989**, *7*, 1–13.

49 A. Grosvenor, B. Kobe, M. Biesinger, N. McIntyre, *Surf. Interface Anal.* **2004**, *36*, 1564–1574.

50 D. Briggs, Handbook of X-Ray Photoelectron Spectroscopy Heyden & Son Ltd.: MN, Minnesota, **1979**; p. 190.

51 R. Paul, R. G. Reifenberger, T. S. Fisher, D. Y. Zemlyanov, *Chem. Mater.* **2015**, *27*, 5915–5924.

52 W. Weiss, W. Ranke, *Prog. Surf. Sci.* **2002**, *70*, 1–151.

53 A. B. F. Martinson, M. J. DeVries, J. A. Libera, S. T. Christensen, J. T. Hupp, M. J. Pellin, J. W. Elam, *J. Phys. Chem. C* **2011**, *115*, 4333–4339.

SUPPORTING INFORMATION

Synthesis and Characterization of Ferrocene Containing Block Copolymers

Sergey Chernyy, *[1] Zhongli Wang,[1,2] Jacob Judas Kain Kirkensgaard,[3] Anders Bakke,[3] Kell Mortensen,[3] Sokol Ndoni,[1,2] Kristoffer Almdal[1,2]

[1]Technical University of Denmark, DTU Nanotech - Department of Micro- and Nanotechnology, Produktionstorvet, 2800 Kgs. Lyngby, Denmark

[2]Center for Nanostructured Graphene, CNG, DTU Nanotech - Department of Micro- and Nanotechnology, Produktionstorvet, 2800 Kgs. Lyngby, Denmark

[3]Niels Bohr Institute, University of Copenhagen, 2100 Copenhagen, Denmark

Correspondence to: Sergey Chernyy (E-mail: *sergeychernyy@gmail.com*)

Contents

SI1. HR XPS of PFMMA before and after TGA

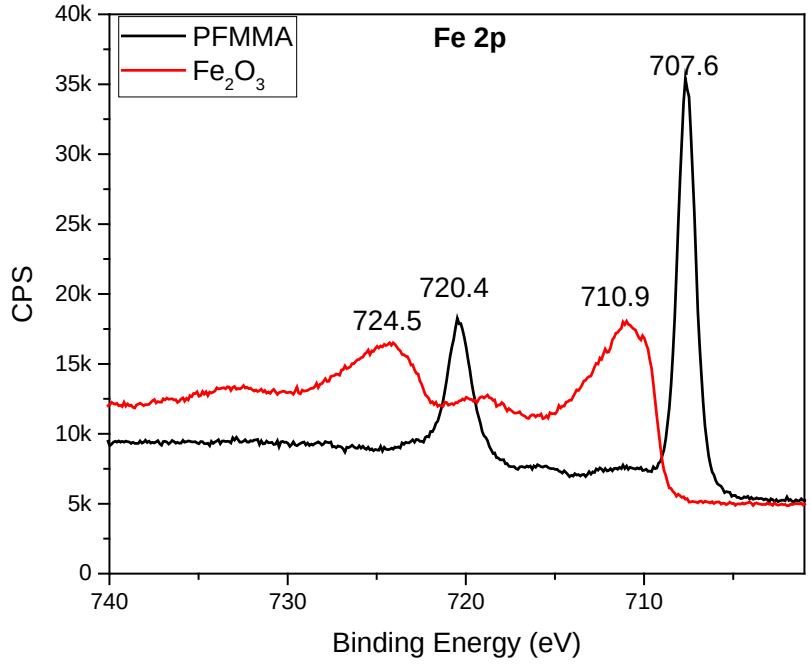

Figure 1. HR XPS spectra of Fe 2p for the PFMMA before (black curve) and after TGA in air (red curve). TGA was recorded at 10°C/min up to 1000 C and the residue was analyzed by XPS immediately after the cooling cycle.

SI2. DSC of PFMMA

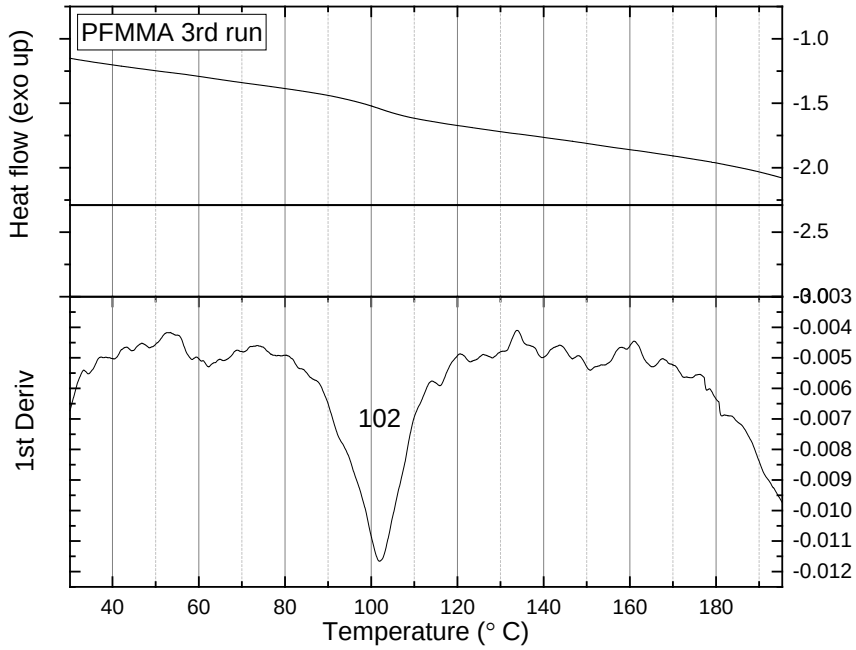

Figure 2. DSC of poly(ferrocenylmethyl methacrylate) recorded at 10°C/min and the corresponding differential curve.

SI3. NMR of PFMMA

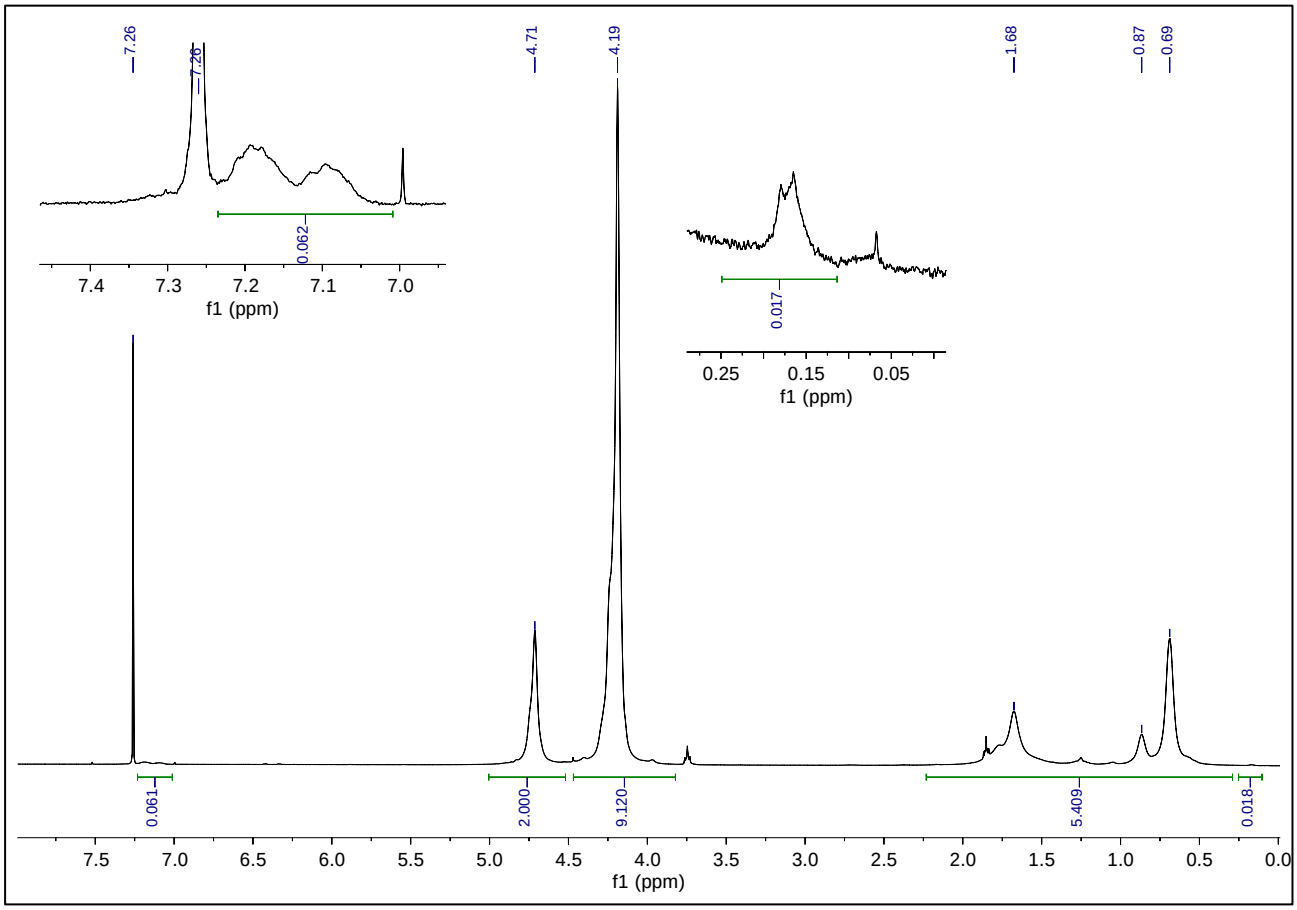

Figure 3. ^{1}H NMR spectra of poly(ferrocenylmethyl methacrylate) in CDCl3, 400 MHz

SI4. TGA of $PF9_{35k}F_{25}$

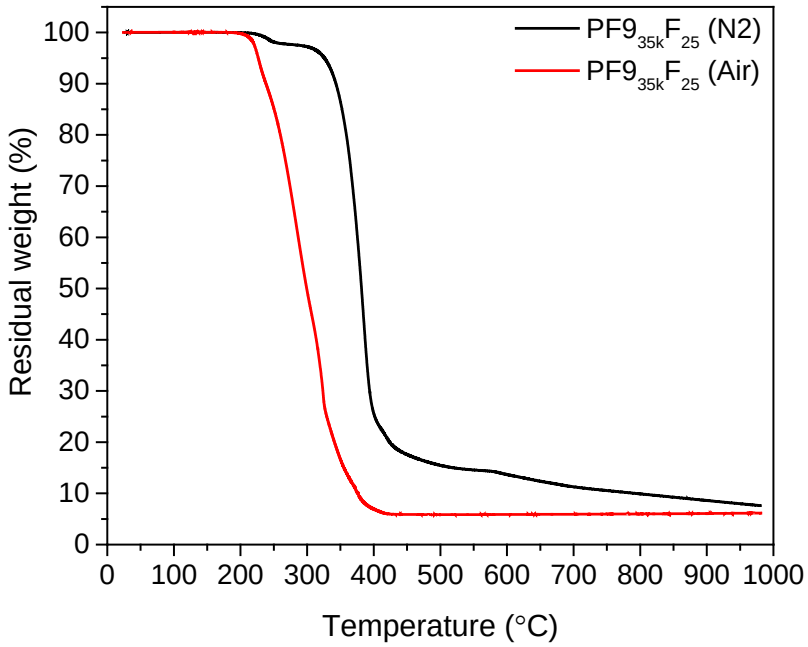

Figure 4. TGA curves of the poly(1*H*,1*H*,2*H*,2*H*-nonafluorohexyl methacrylate-*block*-ferrocenylmethyl methacrylate) in nitrogen and air recorded at 10°C/min

SI5. DSC of $PF9_{35k}F_{25}$

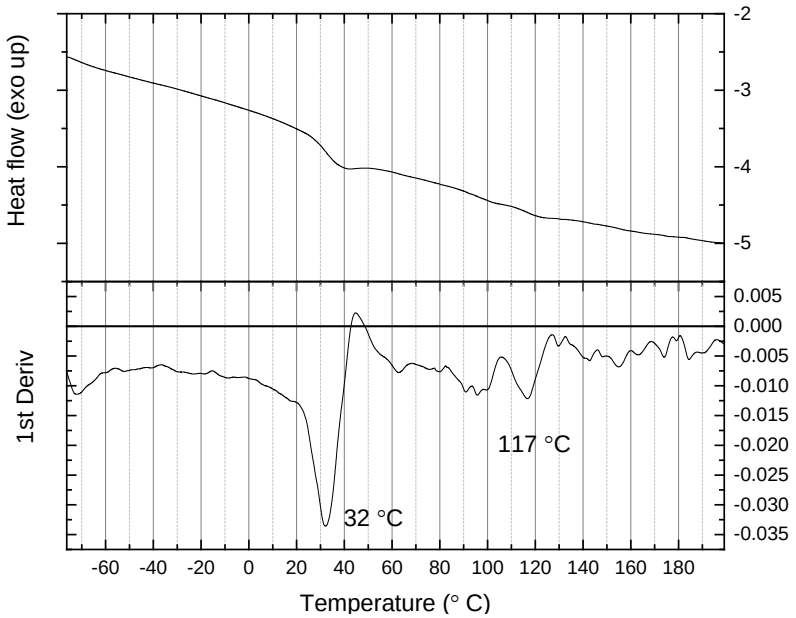

Figure 5. DSC of poly(1*H*,1*H*,2*H*,2*H*-nonafluorohexyl methacrylate-*block*-ferrocenylmethyl methacrylate) recorded at 10°C/min and the corresponding differential curve.

SI6. NMR of $PF9_{35k}F_{25}$

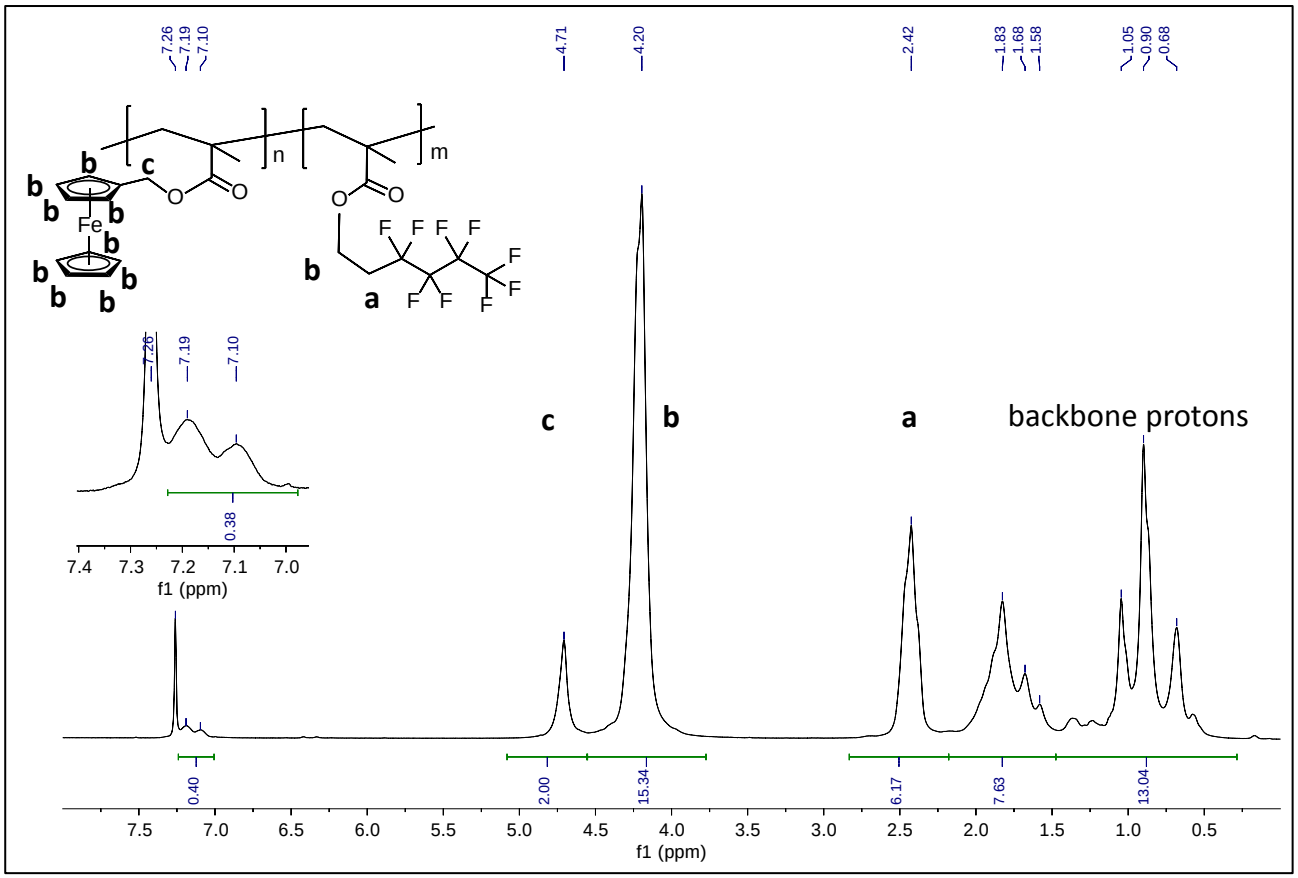

Figure 6. ^{1}H NMR spectra of poly(1*H*,1*H*,2*H*,2*H*-nonafluorohexyl methacrylate-*block*-ferrocenylmethyl methacrylate) [CDCl3, 400 MHz]

SI7. SAXS of $PF9_{35k}F_{25}$

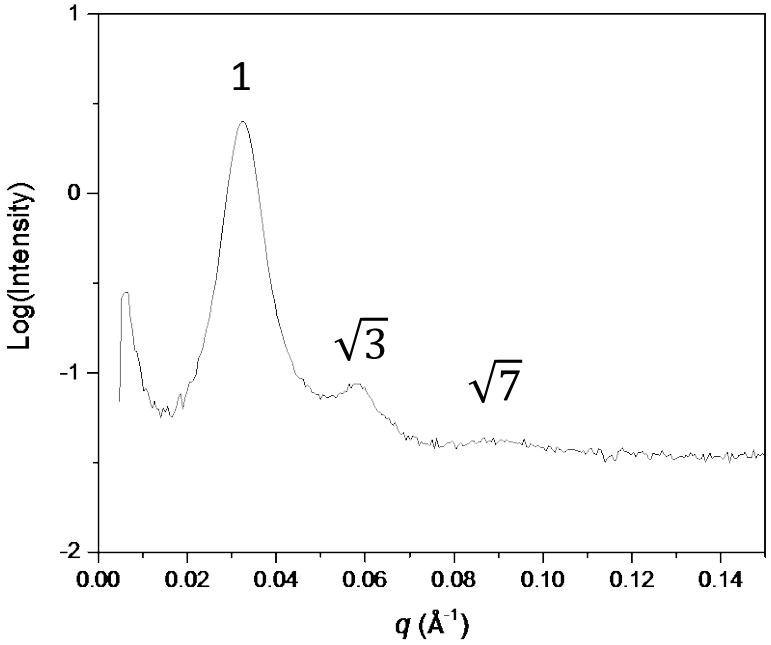

Figure 7. SAXS profile of the poly(1*H*,1*H*,2*H*,2*H*-nonafluorohexyl methacrylate-*block*-ferrocenylmethyl methacrylate) heat annealed for 65 h at 160 °C in vacuum. Peak positions were normalized by the position of the first peak (q*) and their relative peak position ratios q/q^* are designated as $1:\sqrt{3}:\sqrt{7}$ which corresponds to the hexagonally packed cylinder morphology.

SI8. TGA of $PM_{16k}F_{31}$

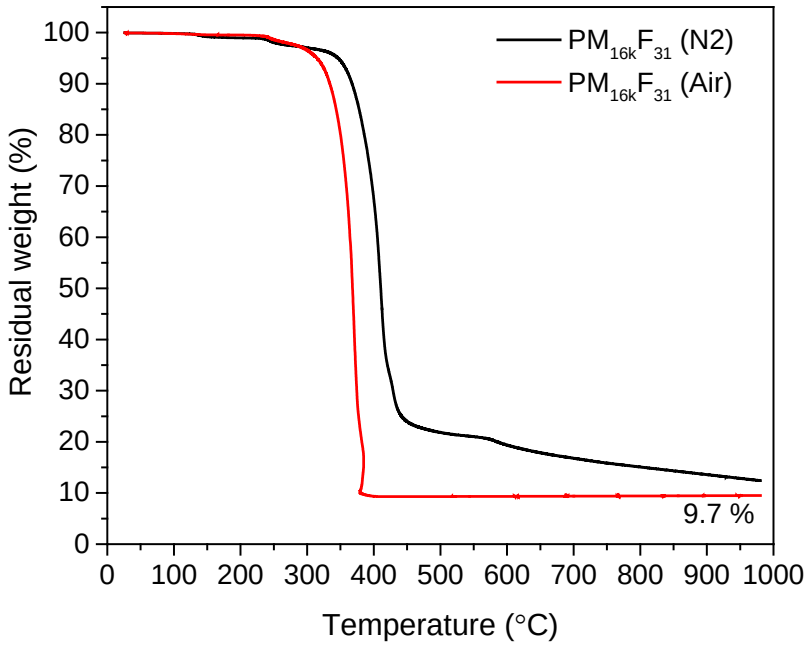

Figure 8. TGA curves of the poly(methyl methacrylate-*block*-ferrocenylmethyl methacrylate) with 31 vol% of PFMMA bock in nitrogen and air recorded at 10°C/min

SI9. DSC of $PM_{16k}F_{31}$

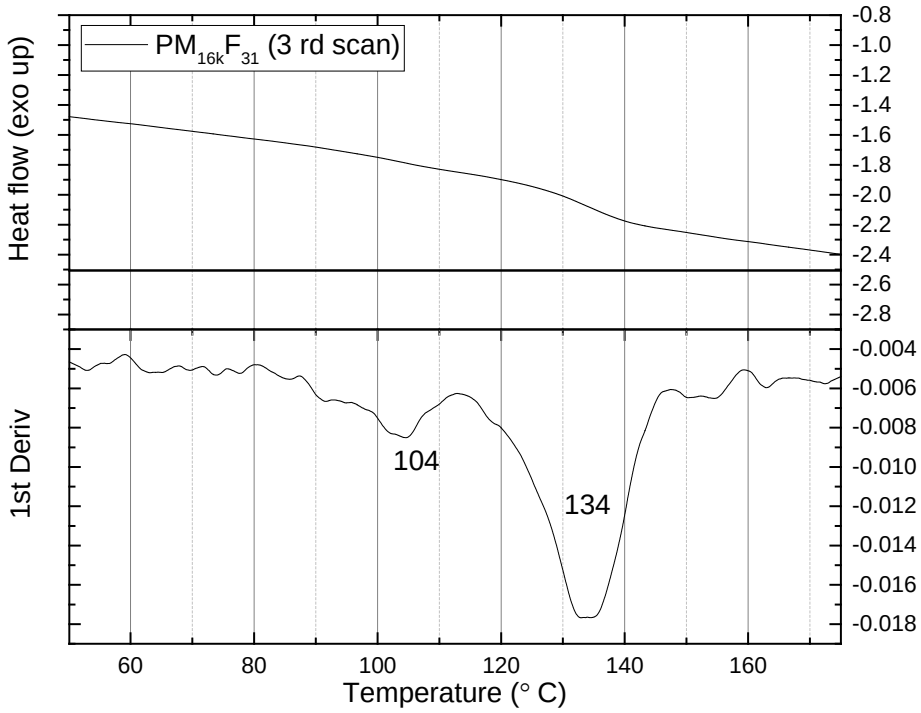

Figure 9. DSC curve of poly(methyl methacrylate-*block*-ferrocenylmethyl methacrylate) with 31 vol% of PFMMA bock recorded at 10°C/min and the corresponding differential curve.

SI10. NMR of $PM_{16k}F_{31}$

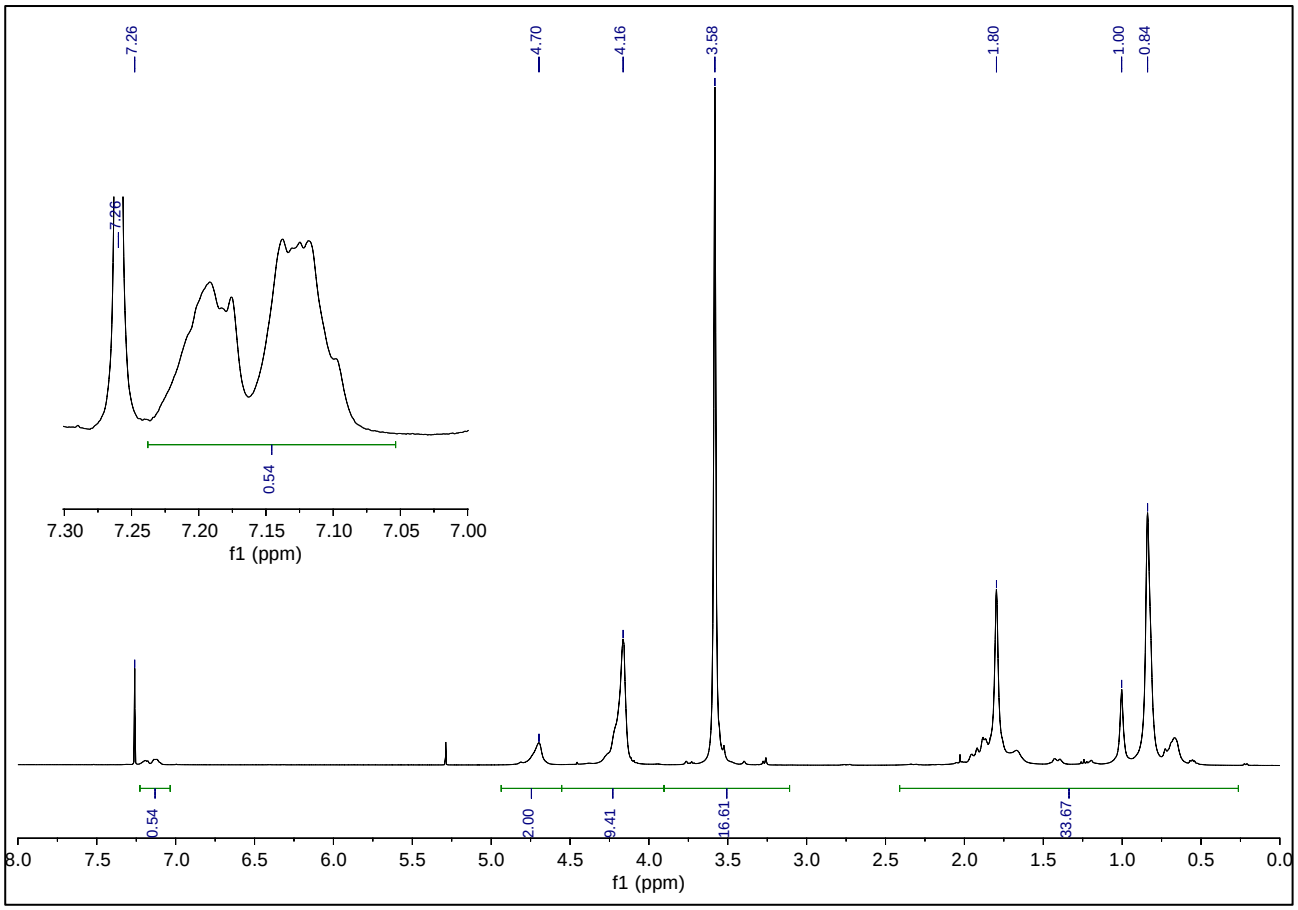

Figure 10. ^{1}H NMR spectra poly(methyl methacrylate-*block*-ferrocenylmethyl methacrylate) with 31 vol% of PFMMA bock (CDCl3, 400 MHz)

SI11. NMR of $PM_{24k}F_{55}$

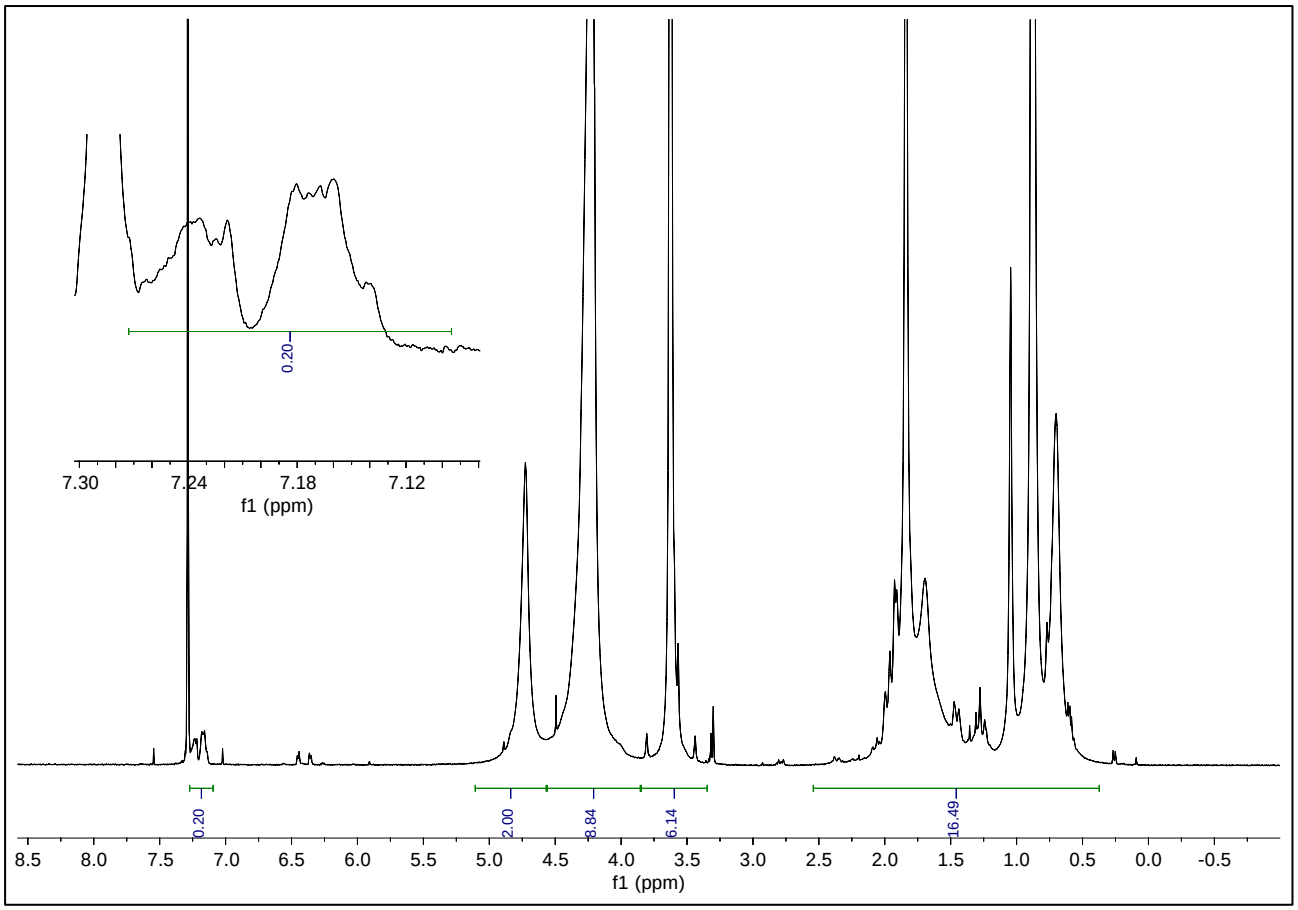

Figure 11. ^{1}H NMR spectra poly(methyl methacrylate-*block*-ferrocenylmethyl methacrylate) with 55 vol% of PFMMA bock (CDCl3, 400 MHz)

SI12. NMR of $PM_{35k}F_{51}$

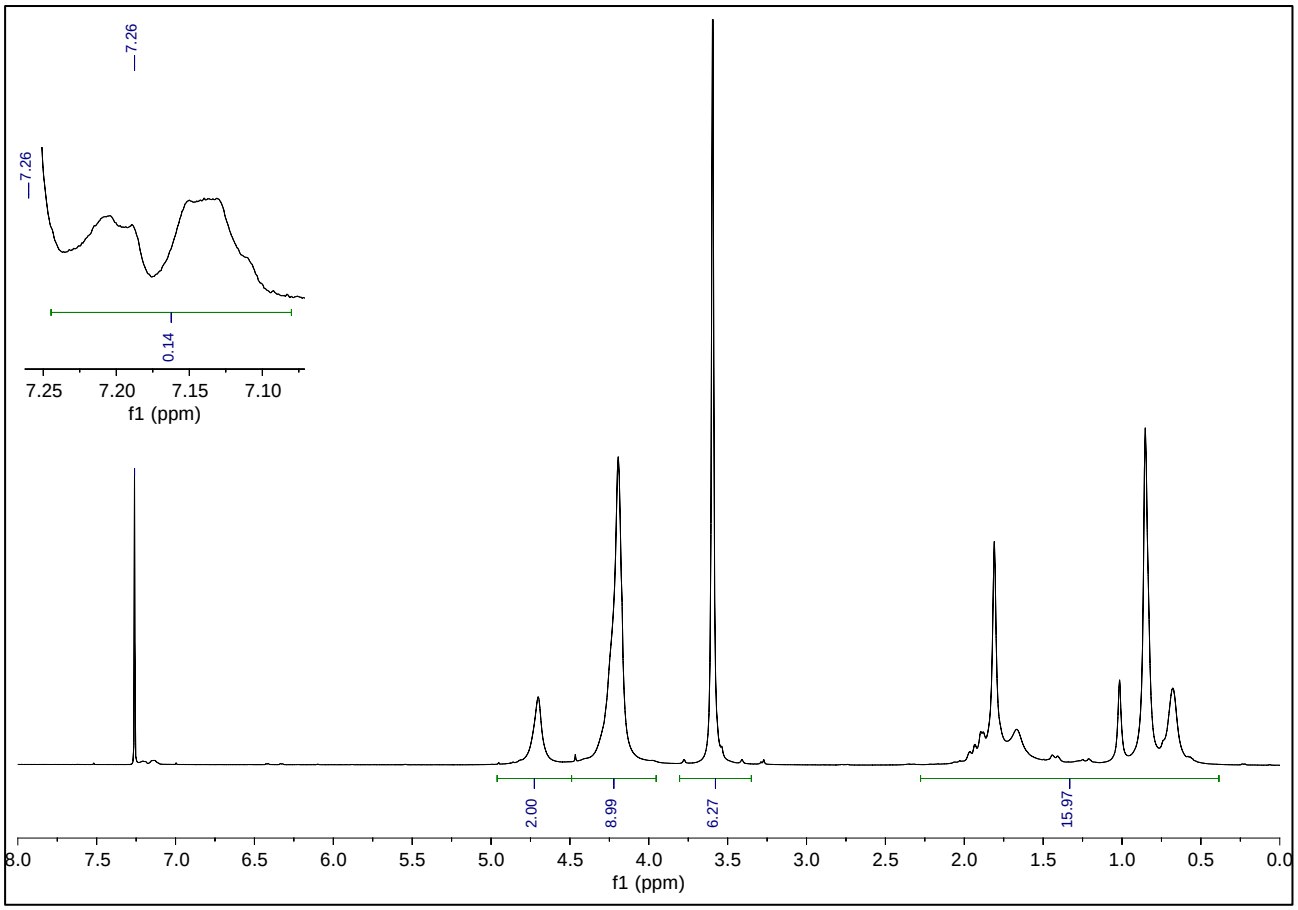

Figure 12. ^{1}H NMR spectra poly(methyl methacrylate-*block*-ferrocenylmethyl methacrylate) with 54 vol% of PFMMA bock (CDCl3, 400 MHz)